

A STATISTICAL FMRI MODEL FOR DIFFERENTIAL T_2^* CONTRAST
INCORPORATING T_1 AND T_2^* OF
GRAY MATTER

By

M. Muge Karaman

A Thesis submitted to the Faculty of the Graduate School,
Marquette University,
in Partial Fulfillment of the Requirements for
the Degree of Master of Science

Milwaukee, Wisconsin

April 2011

ABSTRACT
A STATISTICAL FMRI MODEL FOR DIFFERENTIAL T_2^* CONTRAST
INCORPORATING T_1 AND T_2^* OF
GRAY MATTER

M. Muge Karaman

Marquette University

Relaxation parameter estimation and brain activation detection are two main study areas in magnetic resonance imaging (MRI) and functional magnetic resonance imaging (fMRI). Relaxation parameters can be used to distinguish voxels containing different types of tissue while activation determines voxels that are associated with neuronal activity. In nearly all fMRI studies, the first few scans are discarded from the data before computing brain activation to avoid magnetic saturation effects. However, these first images have important information on the relaxation decay parameters for the type of tissue contained in voxels, which could provide pathological tissue discrimination [3]. It is also well-known that the voxels located in gray matter contain neurons that are to be active while the subject is performing a task and thus voxel relaxivities that are different for different tissue types should be included in a model. In this study, we develop a model to obtain both relaxation parameters and determine brain activation simultaneously. This model is examined with realistically simulated fMRI data, which includes the first few scans as well the remainder of the time series. To compute the activation statistics, the estimated T_1 and T_2^* of gray matter are incorporated into the hypothesis testing setting. Nonlinear least squares estimation is used for estimating the parameters and the general procedure of generalized likelihood ratio test is performed to calculate activation statistics.

ACKNOWLEDGEMENTS

M. Muge Karaman

I would like to express my deepest gratitude to my Advisor, Dr. Rowe, who introduced me to the field of fMRI, for his invaluable guidance and time in this work. I wish to thank Iain Bruce and Andrew Hahn for their helpful suggestions and contributions throughout our research meetings. I also gratefully acknowledge the generous Research Assistantship provided by the Department of Mathematics, Statistics and Computer Science at Marquette University that supported this research.

TABLE OF CONTENTS

ACKNOWLEDGEMENTS.....	i
CHAPTERS	
1. INTRODUCTION.....	1
2. THEORY.....	3
2.1 Relaxation and Magnetization in fMRI	4
2.2 Models.....	6
2.2.1 Complex Activation (CA) Model	6
2.2.2 Magnitude-Only Activation (MO) Model	10
2.2.3 Statistical fMRI Model for Differential T_2^* Contrast (DeTeCT Model)	12
2.2.3.1 Data Generation	12
2.2.3.2 Estimation of Model Parameters	13
2.2.3.3 Activation	15
2.2.4 Statistical fMRI Model for Differential T_2^* Contrast Incorporating T_1 and T_2^* of Gray Matter (DeTeCT-ING Model)	16
2.2.4.1 Data Generation	16
2.2.4.2 Estimation of Model Parameters	16
2.2.4.3 Activation	17
3. fMRI Simulation.....	18
4. Discussion.....	30

1. INTRODUCTION

Functional magnetic resonance imaging (fMRI) is a type of specialized magnetic resonance imaging (MRI) that maps the changes in brain hemodynamics corresponding to neural activity. Magnetic resonance (MR) has the capability of measuring the parameters related to the physiological functions including changes in blood flow, blood volume and blood oxygenation levels in the brain. Blood oxygen level-dependent (BOLD) contrast-based fMRI is a method used to visualize brain functions by measuring the changes in the inhomogeneity of the magnetic field that results from changes in blood oxygenation. Ogawa et al. demonstrated that fMRI could be used to visualize brain activation by measuring the BOLD signal [6].

Magnetic resonance corresponds to the interaction between the applied radio frequency (RF) and the nuclear spin of the hydrogen nuclei (protons) in the brain. These hydrogen atoms radiate energy with the same frequency as the applied RF pulse. The recovery of that nuclear spin magnetization in fMRI follows an exponential decay, which is composed of both longitudinal (T_1) and transverse (T_2^*) relaxation, which will be explained in more detail later.

The data collected during an fMRI experiment is recorded in frequency space, so called k -space, and an inverse Fourier transform is applied to the k -space data in order to obtain images in image-space. In both MRI and fMRI, voxel time measurements after Fourier image reconstruction are complex-valued because of magnetic field inhomogeneities and noise [3]. The reconstructed k -space data are assumed to be corrupted by additive zero mean and uncorrelated Gaussian noise in both the real and imaginary parts.

In fMRI, we seek voxels in which there is a signal increase associated with specific neural activity when a task is performed by the subject. Although many fMRI studies obtain a statistical measure of functional activation based on magnitude-only image time courses,

discarding the phase component, Rowe and Logan illustrated that the complex-valued activation model has superior power in detecting activation over that of the standard magnitude-only activation model [7,8]. Therefore, the statistical fMRI model for detecting activation introduced in this manuscript is based upon the complex-valued activation model of Rowe and Logan, and will be briefly summarized in the next section.

The quantification of T_1 and T_2^* relaxation times and spin density has become a popular area of study in the field of fMRI as being a fundamental way of characterizing the tissue contained within each voxel since they are not affected by different machine settings. Knowledge of the relaxation parameters within a voxel can be used to reduce the number of voxels declared active that have partial voluming (part of their volume occupied by grey matter and part of their volume occupied by another type of tissue). Using only the magnitude of complex-valued magnetic resonance images has become the gold standard for the estimation of the relaxation parameters [4]. However, Baselice et al. recently utilized complex-valued images for relaxation parameter estimation [1]. Also, least squares estimation has become a commonly used technique for estimating the relaxation parameters.

In this manuscript, we expand upon previous models by proposing a statistical fMRI model that uses complex-valued time courses to simultaneously estimate the relaxation parameters (T_1 and T_2^*) and to detect brain activation, which has been incorporated into the model by a differential T_2^* contrast parameter δ . The tissue parameters T_1 and T_2^* are estimated from theoretically simulated fMRI data, where the first few scans of the brain are not discarded, unlike the common practice of conventional studies. Nonlinear least squares, which is one of the most common techniques for parameter estimation, is used for simultaneously obtaining the relaxation parameters of different tissues and estimating activation model parameters. We will utilize a single pulse sequence with three parts, where in the first two parts the subject does not perform the task while in the third part the subject performs the task as in a standard fMRI

experiment. In the first part, several images are acquired at a constant echo time; in the second part, the echo time is varied; and in the third part the echo time is constant. This pulse sequence allows us to have the three parts for: a) T_1 estimation, b) T_2^* estimation and c) detecting activation, while all of the model parameters are estimated simultaneously using data from the entire scan. For detecting activation, maximum likelihood estimators are numerically calculated under both the restricted null and unrestricted alternative hypotheses. As the active voxels are located in gray matter, both the T_1 and T_2^* values of gray matter are included in the hypothesis testing setup in such a way so that the voxels located in gray matter can be detected. Activation statistics are derived from the generalized likelihood ratio test and thresholded activation maps are obtained from a 5% Bonferroni family-wise-error rate (FEW) thresholding technique [8, 17].

The main advantage of this model is that it provides a practical technique for relaxation parameter estimation and detecting brain activation by obtaining these parameters simultaneously from the correct physical model. It also makes use of the generally discarded TR images at the beginning of the time series, which in fact contain important biological information on various tissue types in the brain. To the best of our knowledge, this study is the first to detect brain activation by incorporating simultaneously estimated T_1 and T_2^* values of the gray matter. As such, the model outlined in this manuscript contributes to the field by quantifying the activation statistics in a more accurate and informed way.

2. THEORY

In fMRI, the measured signal is a combination of the total number of nuclei (proton spin density) reduced by the T_1 and T_2^* relaxation components. Further, we obtain a complex-valued measurement of the object plus complex-valued noise after image reconstruction. In this section, the role of the relaxation decay times in fMRI will be briefly summarized; and the commonly used fMRI magnitude-only activation model [15,16] along with the more recent complex-valued

activation model [8] will be presented. Our advanced statistical fMRI models, built upon the existing complex-valued fMRI activation model of Rowe and Logan (2004) with the enhancement of simultaneously determining the relaxation parameters and the differential T_2^* contrast, will also be introduced. The numerical and statistical methods which will be used to estimate the relaxation parameters and determine the brain activation will also be described.

2.1 Relaxation and Magnetization in fMRI

In MRI/fMRI, when a brief radio frequency is applied, the hydrogen atoms absorb energy (excitation) and their equilibrium state is perturbed. These hydrogen atoms emit energy which is called the relaxation process and then they return from the tipped state to their original lower energy state of being aligned in the direction of the magnetic field. The characteristic times involved in the relaxation of the nuclear spin magnetization vector, M , are known as relaxation times. Longitudinal, or spin-lattice, relaxation time, T_1 , is the decay constant for the recovery of the z component of the magnetization, M_z , towards its thermal equilibrium value, $M_{z,eq}$. The transverse, or spin-spin, relaxation time, T_2 , is the decay constant for the component of M perpendicular to external magnetic field, B_0 , designated M_{xy} . While all hydrogen nuclei in a magnetic field precess with the same frequency in an ideal system, there is an additional dephasing of the magnetization introduced by external field inhomogeneities. This reduction in the initial value of M_{xy} can be characterized by a separate decay time, T_2^* , which is the decay parameter for the magnetization including both T_2 from completely random interaction between spins and magnetic field inhomogeneities B_0 [3].

The inhomogeneity of the magnetic field is considered to be an artifact, and despite many efforts to make the overall magnetic field as uniform as possible, local magnetic field susceptibility differences between brain tissue are still present.

The changes in blood oxygenation cause changes in magnetic field inhomogeneity and thus in decay parameter T_2^* , as the T_2^* signal is relatively sensitive to inhomogeneities in the magnetic field. This leads to changes in image intensity in T_2^* -weighted images, which are thus used to study brain activity in brain functional imaging studies [5].

The spin density and relaxation times provide the three most intrinsic and basic contrast mechanisms in MRI/fMRI. It is thus of interest to measure and exploit differences in these parameters in order to develop image contrast between different brain tissue since the resulting measured values could be used for tissue characterization and provide useful information on local environment interaction. The quantization of the relaxation parameters helps to both predict the signal-to-noise ratio (SNR) and contrast-to-noise ratio (CNR) for a given sequence and makes it possible to better understand the contrast mechanism and the tissue characterization.

The Bloch equations describe the behavior of a magnetization vector in the presence of an externally applied magnetic field subject to the relaxation process [3]. According to the solution of the Bloch equations, magnetization can be characterized by the tissue parameters (T_1 , T_2 or T_2^* , M_0) and imaging parameters (TR , TE , ϕ) where M_0 is the spin density, TR is the repetition time, TE is the echo time and ϕ is the flip angle. Thus, the signal change can be induced by a change in spin density, T_1 , and/or T_2^* . In a T_2^* -weighted gradient echo (GRE) fMRI experiment, for a stationary voxel, the magnetization after the t^{th} excitation, M_t , for a series of excitations with a repetition time of TR , echo time TE_t and flip angle of ϕ is given by:

$$M_t = \left[M_{t-1} e^{-\frac{TR}{T_1}} \cos(\phi) + M_0 \left(1 - e^{-\frac{TR}{T_1}} \right) \right] \sin(\phi) e^{-\frac{TE_t}{T_2^*}}. \quad (1)$$

2.2 Models

In this section, the two commonly used fMRI activation models: magnitude-only [15,16] and complex-valued [8,16] fMRI activation model are described. Then, our proposed statistical fMRI activation model for T_2^* contrast without incorporating the relaxation parameter values of gray matter is introduced. Lastly, we present a further improved model that includes the relaxation parameters of gray matter are into the model that estimates the activation parameter and activation statistics.

2.2.1 Complex Activation (CA) Model

As previously noted, an RF pulse is used to tip the aligned hydrogen nuclei to construct an image within a slice of the brain. The nuclei then return to their original aligned positions by inducing a current in a receiver coil, which provides the basic MR signal. Each measurement of the signal can be approximately expressed as the Fourier transformation of the spin density at a single point in the frequency domain (k -space). In MRI/fMRI, the signal is corrupted by additive thermal noise whose standard source is the human subject, as the human body itself generates electromagnetic noise due to its structure that is comprised of ions and electrons. Other sources of noise and unwanted signal can be from the reception coil, the analog to digital conversion, and movement of the subject such as chest movement, respiration and head movement. Thus, the raw k -space data is complex-valued, and it is assumed that both the real and imaginary components are measured with independent normally distributed error.

In order to obtain MR images in the spatial domain, an inverse Fourier transform, which is a linear and orthogonal operation, is required. After the inverse Fourier transform, images or voxel measurements are complex-valued and still corrupted by noise in both real and imaginary

parts. The magnitude of a complex-valued observation at time t is Ricean distributed and can be approximated by the normal distribution at high SNR [7,9,10].

The complex-valued image measured over time in a given voxel is:

$$y_t = (M_t \cos \theta_t + \eta_{R_t}) + i(M_t \sin \theta_t + \eta_{I_t}), \quad (2)$$

$$t = 1, \dots, n$$

where $(\eta_{R_t}, \eta_{I_t})' \sim N(0, \sigma^2 I_2)$, the true population magnitude is M_t and the phase is θ_t .

The data gathered during the course of an fMRI experiment is comprised of a sequence of individual MR images acquired while the subject performs a set of tasks. Throughout the experiment, the subject alternates between remaining still and performing a task allowing the task-related activations to be detected by qualifying the relative changes in the measured signal between individual images. The task-related activations are detected by qualifying the relative changes in the measured signal between individual images. Using periods of non-task scans is a common means of establishing a baseline on which the assumption is made that the brain activity scales in a linear fashion. A linear model is generally used to describe the temporally varying magnitude M_t :

$$M_t = x_t' \beta = \beta_0 + \beta_1 x_{1t} + \dots + \beta_q x_{qt}, \quad (3)$$

where x_t is the t^{th} row of an $n \times (q + 1)$ design matrix X , and β is a $(q + 1) \times 1$ vector of magnitude regression coefficients. Thus, the observed complex-valued data at time t can be represented by a 2×1 real-valued vector,

$$\begin{pmatrix} y_{R_t} \\ y_{I_t} \end{pmatrix} = \begin{pmatrix} x'_t \beta \cos \theta_t \\ x'_t \beta \sin \theta_t \end{pmatrix} + \begin{pmatrix} \eta_{R_t} \\ \eta_{I_t} \end{pmatrix},$$

$$t = 1, \dots, n, \quad (4)$$

where y_{R_t} is the real part and y_{I_t} is the imaginary part. This is a very general linear multiple regression model.

This model can also be written more generally as

$$y = \begin{pmatrix} X & 0 \\ 0 & X \end{pmatrix} \begin{pmatrix} \beta \cos \theta \\ \beta \sin \theta \end{pmatrix} + \eta$$

$$2n \times 1 \quad 2n \times 2(q+1) \quad 2(q+1) \times 1 \quad 2n \times 1$$

where the observed vector of data $y = (y'_R, y'_I)'$ is the vector of observed real values stacked on the observed imaginary values and the vector of errors $\eta = (\eta'_R, \eta'_I)' \sim N(0, \Sigma \otimes \Phi)$ is similarly defined. It is generally assumed that $\Sigma = \sigma^2 I_2$ and $\Phi = I_n$.

Recall that fMRI does not directly measure the electrical activity of the neurons, but the change in blood oxygenation indirectly caused by that activity. Thus, model parameters are estimated under the appropriately constrained null and alternative hypotheses, $H_0: C\beta = 0$ versus $H_1: C\beta \neq 0$, after which activation is determined with a generalized likelihood ratio statistic.

Unrestricted MLE's of the parameters can be derived as

$$\begin{aligned}
\hat{\theta} &= \frac{1}{2} \tan^{-1} \left[\frac{2\hat{\beta}'_R (X'X) \hat{\beta}_I}{\hat{\beta}'_R (X'X) \hat{\beta}_R - \hat{\beta}'_I (X'X) \hat{\beta}_I} \right] \\
\hat{\beta} &= \hat{\beta}_R \cos \hat{\theta} + \hat{\beta}_I \sin \hat{\theta} \\
\hat{\sigma}^2 &= \frac{1}{2n} \left[y - \begin{pmatrix} X \hat{\beta} \cos \hat{\theta} \\ X \hat{\beta} \sin \hat{\theta} \end{pmatrix} \right]' \left[y - \begin{pmatrix} X \hat{\beta} \cos \hat{\theta} \\ X \hat{\beta} \sin \hat{\theta} \end{pmatrix} \right]
\end{aligned} \tag{5}$$

where $\hat{\beta}_R = (X'X)^{-1} X'y_R$ and $\hat{\beta}_I = (X'X)^{-1} X'y_I$.

The MLE's under the constrained null hypothesis $H_0 : C\beta = 0$ can also be derived as

$$\begin{aligned}
\tilde{\theta} &= \frac{1}{2} \tan^{-1} \left[\frac{2\hat{\beta}'_R \Psi (X'X) \hat{\beta}_I}{\hat{\beta}'_R \Psi (X'X) \hat{\beta}_R - \hat{\beta}'_I \Psi (X'X) \hat{\beta}_I} \right] \\
\tilde{\beta} &= \Psi \left[\hat{\beta}_R \cos \tilde{\theta} + \hat{\beta}_I \sin \tilde{\theta} \right] \\
\tilde{\sigma}^2 &= \frac{1}{2n} \left[y - \begin{pmatrix} X \tilde{\beta} \cos \tilde{\theta} \\ X \tilde{\beta} \sin \tilde{\theta} \end{pmatrix} \right]' \left[y - \begin{pmatrix} X \tilde{\beta} \cos \tilde{\theta} \\ X \tilde{\beta} \sin \tilde{\theta} \end{pmatrix} \right],
\end{aligned}$$

where

$$\Psi = I_{q+1} - (X'X)^{-1} C' [C(X'X)^{-1} C']^{-1} C. \tag{6}$$

Denoting the maximum likelihood estimators under the alternative hypothesis using hats, and those under the null hypothesis using tildes, the generalized likelihood ratio statistic can be derived as,

$$-2 \log \lambda_C = 2n \log \left(\frac{\tilde{\sigma}^2}{\hat{\sigma}^2} \right). \tag{7}$$

This statistic under the null hypothesis is approximately χ_r^2 distributed in large samples, where r is the difference in the number of constraints between the alternative and the null

hypotheses or the full row rank of C . This statistic is asymptotically equivalent to the usual t or F tests associated with statistical parametric maps. For the complex activation model with β_0 representing an intercept, β_1 representing a linear drift over time, and β_2 representing a contrast effect of a stimulus, we test whether the coefficient for the reference function is 0 by setting $C = (0,0,1)$ so that the hypothesis is $H_0: \beta_2 = 0$. Note that, when $r = 1$, two-sided testing can be performed using the signed likelihood ratio test [8,13] given by

$$Z_C = \text{sign}(C\hat{\beta})\sqrt{-2\log \lambda_C} \quad (8)$$

2.2.2 Magnitude-Only (MO) Activation Model

In fMRI, complex-valued time courses are almost exclusively converted to magnitude and phase time courses, then the magnitude-only activation is detected while phase voxel time courses are discarded [11,12]. This typical method to compute the activation using only the magnitude at time t , denoted by m_t and written as

$$m_t = \left[\left(M_t \cos \theta_t + \eta_{R_t} \right)^2 + \left(M_t \sin \theta_t + \eta_{I_t} \right)^2 \right]^{\frac{1}{2}}, \quad (9)$$

where $(\eta_{R_t}, \eta_{I_t})' \sim N(0, \sigma^2 I_2)$ and true population magnitude, M_t , is given by Eq. (3).

The magnitude-only model in Eq. (9) discards any information on the phase, which is given by

$$\varphi_t = \tan^{-1} \left[\frac{M_t \sin \theta_t + \eta_{I_t}}{M_t \cos \theta_t + \eta_{R_t}} \right]. \quad (10)$$

The magnitude of a complex-valued observation at time t is not normally distributed but is Ricean distributed [8,9,10]. The Ricean distribution of the magnitude m_t is approximately normal with mean $x_t'\beta$ and variance σ^2 at high SNRs.

This model can also be written as

$$\begin{matrix} m & = & X & \beta & + & \varepsilon \\ n \times 1 & & n \times (q+1) & (q+1) \times 1 & & n \times 1 \end{matrix} \quad (11)$$

where $\varepsilon \sim N(0, \sigma^2 \Phi)$, Φ is the temporal correlation matrix often taken to be $\Phi = I_n$ after pre-whitening of the data, n is the number of time points and q is the number of non-baseline regressors [8].

The unconstrained maximum likelihood estimates of the parameters (β, σ^2) can be derived as

$$\begin{aligned} \hat{\beta} &= (X'X)^{-1} X'm \\ \hat{\sigma}^2 &= (m - X\hat{\beta})'(m - X\hat{\beta})/n. \end{aligned} \quad (12)$$

In order to construct a generalized likelihood ratio test of the hypothesis $H_0: C\beta = 0$ versus $H_1: C\beta \neq 0$, where C is a full row rank matrix, the likelihood under the constrained hypothesis is maximized. The constrained MLE's can be derived as

$$\begin{aligned} \tilde{\beta} &= \Psi \hat{\beta} \\ \tilde{\sigma}^2 &= (m - X\tilde{\beta})'(m - X\tilde{\beta})/n, \end{aligned} \quad (13)$$

where Ψ is defined as in Eq. (6).

Similarly with the complex activation model, the likelihood ratio statistic for the magnitude-only model is given by,

$$-2 \log \lambda_M = n \log \left(\frac{\tilde{\sigma}^2}{\hat{\sigma}^2} \right). \quad (14)$$

The likelihood ratio statistic under the null hypothesis has an asymptotic χ_1^2 distribution and with algebra the usual t tests for activation can be derived, given by

$$t_2 = \frac{\hat{\beta}_2}{SE(\hat{\beta}_2)}. \quad (15)$$

2.2.3 Statistical fMRI Model for Differential T_2^* Contrast (DeTeCT Model)

This model differs from previously described activation models because it describes the physical process that has generated the data. The fMRI data is generated according to the equation of the temporally varying magnitude of the signal where the differential T_2^* contrast is also included to model the activation. The model parameters are determined by using Least Squares (LS) estimation and activation statistics is calculated by performing the general procedure of generalized likelihood ratio test. In the rest of the manuscript, this model will be called the “DeTeCT Model”, where “D” stands for “Differential”, “T” stands for “Transverse relaxation, T_2^* ” and “CT” stands for “Contrast”.

2.2.3.1 Data Generation

As previously noted, the measured MR signal decays over time depending on the relaxation times and the spin density of the given voxel. The fMRI voxel measurements are a sequence of individual MR signals which are taken when the subject is performing a previously

explained task for a particular period of time, and then not performing for the next period of time. The temporally varying magnitude of the signal can be represented by incorporating the effect of the task execution to the magnetization. In this manuscript, the temporally varying magnitude, M_t , for an individual voxel, is defined as

$$M_t = \left[M_{t-1} e^{-\frac{TR}{T_1}} \cos(\phi) + M_0 \left(1 - e^{-\frac{TR}{T_1}} \right) \right] \sin(\phi) e^{-\frac{TE_t}{T_2^* + \delta z_t}} + x_t \beta_1. \quad (16)$$

where $x_t' \beta_1 = \beta_1 x_t$.

In this model, δ is the differential signal change, which is a coefficient for a reference function z_t related to a block experimental design. As we noted before, brain activation causes changes in blood oxygenation leading to changes in decay parameter, T_2^* , and thus the image intensity in T_2^* -weighted images. Therefore, the parameter δz_t is included with the decay parameter T_2^* in the exponential function. The coefficient β_1 is the coefficient for a time trend t for all voxels.

The complex-valued observations at time t can be described as

$$y_t = M_t (\cos \theta_t + i \sin \theta_t) + (\eta_{R_t} + i \eta_{I_t}) \quad (17)$$

$$t = 1, \dots, n,$$

where M_t is given by Eq. (16) and $(\eta_{R_t}, \eta_{I_t})' \sim N(0, \sigma^2 I_2)$.

2.2.3.2 Estimation of Model Parameters

In this model, we focus on the estimation of the differential T_2^* contrast δ and the time trend coefficient β_1 of the individual voxels from the generated complex-valued fMRI data. The

relaxation parameters, T_1 and T_2^* , the phase, θ and the spin density, M_0 , values of the voxels are assumed to be known.

As previously stated, the observed fMRI signal is complex-valued and the probability distributions of the real and imaginary parts of the given signal are normally distributed. Moreover, Least Squares (LS) estimation is a method of estimating parameters by minimizing the squared discrepancies on the observed data and their expected values. Working in the complex domain with the data having normally distributed noise and dealing with an over determined system allows for the use of a LS estimator, which is a computationally convenient measure of fit. As the unknown parameters of this model, $(M_0, T_1, T_2^*, \delta, \beta, \theta)$ are nonlinear in the representation of the signal given by Eq. (16), a nonlinear LS estimation is implemented.

The nonlinear LS estimator, $\hat{\Gamma}(M_0, T_1, T_2^*, \delta, \beta, \theta)$ is obtained by minimizing the function,

$$\sigma^2(M_0, T_1, T_2^*, \delta, \beta, \theta | y_R, y_I, TR, \phi, TE_t, z_t) = \frac{1}{2n} \sum_{t=1}^n [(y_R - M_t \cos \theta)^2 + (y_I - M_t \sin \theta)^2] \quad (18)$$

with respect to the unknown parameters, $M_0, T_1, T_2^*, \delta, \beta, \theta$; where M_t is given by Eq. (16). In this objective function, $y_t = y_R + iy_I$ is the observed signal of an individual voxel at time t ; and $M_t \cos \theta$ and $M_t \sin \theta$ are the expected real and imaginary parts of the signal.

It is well known that the LS procedure corresponds to the maximum likelihood estimate (MLE) when appropriate probabilistic assumptions about underlying error distributions can be made, as in the proposed model. Since the nonlinear LS problem has no closed form solution and is usually solved by iterative refinement, the parameters of the model in this manuscript will be determined numerically.

2.2.3.3 Activation

The main issue in analyzing functional MRI images is comparing images in a statistically meaningful way. In this manuscript, the simple matter of detecting ‘activation’, the local increase in the effect of the task, with most of the brain unaffected by the task, is the primary focus of study. The model parameters are estimated under appropriately constrained null and unconstrained alternative hypotheses, after which activation is determined, which is characterized by differential T_2^* contrast, δ , with a generalized likelihood ratio statistic.

According to the parameterization in this setting, “active” or “on” regions in the brain contain voxels with values $\delta \neq 0$ while “inactive” or “off” regions contain voxels with $\delta = 0$. Maximum likelihood estimates of the parameters $(M_0, T_1, T_2^*, \delta, \beta, \theta)$ can be determined for both restricted alternative and null hypotheses. The hypotheses pair,

$$H_0 : \delta = 0 \text{ versus } H_1 : \delta \neq 0 \quad (19)$$

detect task related voxel activation. Parameter estimates under the null hypothesis,

$(\tilde{M}_0, \tilde{T}_1, \tilde{T}_2^*, \tilde{\delta}, \tilde{\beta}, \tilde{\theta})$ and the alternative hypothesis, $(\hat{M}_0, \hat{T}_1, \hat{T}_2^*, \hat{\delta}, \hat{\beta}, \hat{\theta})$ were both determined by numerical minimization of Eq. (18) with respect to the parameters. The generalized likelihood ratio statistics, λ , the ratio of the likelihoods with restricted null and alternative hypotheses parameter estimates inserted leads to the large sample χ_1^2 distributed statistic $-2 \log \lambda_c$ that is given in Eq. (7). Two-sided testing has been performed using the signed likelihood ratio test which is given by Eq. (8).

2.2.4 Statistical fMRI Model for Differential T_2^* Contrast Incorporating T_1 and T_2^* of Gray

Matter (DeTeCT-ING Model)

In this proposed model, we obtain both relaxation parameters and determine fMRI activation by incorporating T_1 and T_2^* of gray matter with the idea that active voxels in brain are located in gray matter. We differentiate this model from the DeTeCT Model, by including the relaxation parameter values of gray matter into activation statistics. Therefore, we include the suffix “-ing”, which stands for “Incorporating GM” into the name of the model.

2.2.4.1 Data Generation

In this model, the complex-valued observations at time t are generated according to Eq. (16), similarly with the DeTeCT Model.

2.2.4.2 Estimation of Model Parameters

Here, we concentrate on simultaneous estimation of the relaxation parameters, T_1 and T_2^* ; and the differential T_2^* contrast of the individual voxels from the generated fMRI data. As previously noted, the nonlinear unknown parameters can be estimated by implementing nonlinear LS estimation which corresponds to the MLE for our model. The estimation of the parameters $M_0, T_1, T_2^*, \delta, \beta$ and θ for the proposed model is as follows.

The nonlinear LS estimator, $\hat{\Phi}(M_0, T_1, T_2^*, \delta, \beta, \theta)$ is obtained by minimizing the function,

$$\sigma^2(M_0, T_1, T_2^*, \delta, \beta, \theta | y_{R_t}, y_{I_t}, TR, \phi, TE_t, z_t) = \frac{1}{2n} \sum_{t=1}^n [(y_{R_t} - M_t \cos \theta)^2 + (y_{I_t} - M_t \sin \theta)^2] \quad (20)$$

with respect to the unknown parameters, $M_0, T_1, T_2^*, \delta, \beta, \theta$; where M_t is given by Eq. (16). In this objective function, $y_t = y_{R_t} + iy_{I_t}$ is the observed signal of an individual voxel at time t ; and $M_t \cos \theta$ and $M_t \sin \theta$ are the expected real and imaginary parts of the signal.

2.2.4.3 Activation

The model parameters are estimated under appropriately constrained null and alternative hypotheses, after which activation is determined, which is characterized by differential T_2^* contrast, δ , with a generalized likelihood ratio statistic. Unlike the DeTeCT Model, we incorporate T_1 and T_2^* values of the gray matter into the hypothesis testing. Here, it has been taken into the consideration that the neural activations are controlled by the voxels in gray matter of the brain. According to the parameterization in this setting, “active” or “on” regions in the brain contain voxels with values $T_1 = T_{1_{GM}}, T_2^* = T_{2_{GM}}^*$ and $\delta \neq 0$ while “inactive” or “off” regions contain voxels with $T_1 = T_{1_{GM}}, T_2^* = T_{2_{GM}}^*$ and $\delta = 0$ where $T_{1_{GM}}$ and $T_{2_{GM}}^*$ are the T_1 and T_2^* values of the gray matter.

Maximum likelihood estimates of the parameters $(M_0, T_1, T_2^*, \delta, \beta, \theta)$ can be determined for both restricted alternative and null hypotheses. The hypotheses pair,

$$H_0 : T_1 = T_{1_{GM}}, T_2^* = T_{2_{GM}}^*, \delta = 0 \text{ vs. } H_1 : T_1 = T_{1_{GM}}, T_2^* = T_{2_{GM}}^*, \delta \neq 0 \quad (21)$$

detect task related voxel activation. Parameter estimates under the null hypothesis, $(\tilde{M}_0, \tilde{T}_1, \tilde{T}_2^*, \tilde{\delta}, \tilde{\beta}, \tilde{\theta})$ and the alternative hypothesis, $(\hat{M}_0, \hat{T}_1, \hat{T}_2^*, \hat{\delta}, \hat{\beta}, \hat{\theta})$ were both determined by numerical minimization of Eq. (20) with the respective parameters. The generalized likelihood ratio statistics, λ_c , leads to the large sample χ_1^2 distributed statistic $-2 \log \lambda_c$ that is given in Eq.

(7). The signed likelihood ratio test given by Eq. (8) has been used for two-sided testing similarly with the DeTeCT Model.

3. FMRI SIMULATION

Data for all of the models introduced was generated to simulate voxel activation from a bilateral finger tapping fMRI block design experiment according to the regarding models. The block design consisted of 20 s off followed by sixteen epochs of 15 s on and 15 s off with an observation interval of 1 s or a $TR = 1000$ ms.

Before applying the complex and magnitude-only activation models to the simulated data, the first 20 observations were excluded as common practice in fMRI studies. Unlike traditional studies, these first observations were not discarded in the DeTeCT and DeTeCT-ING Models as they contain information on different tissue characterization.

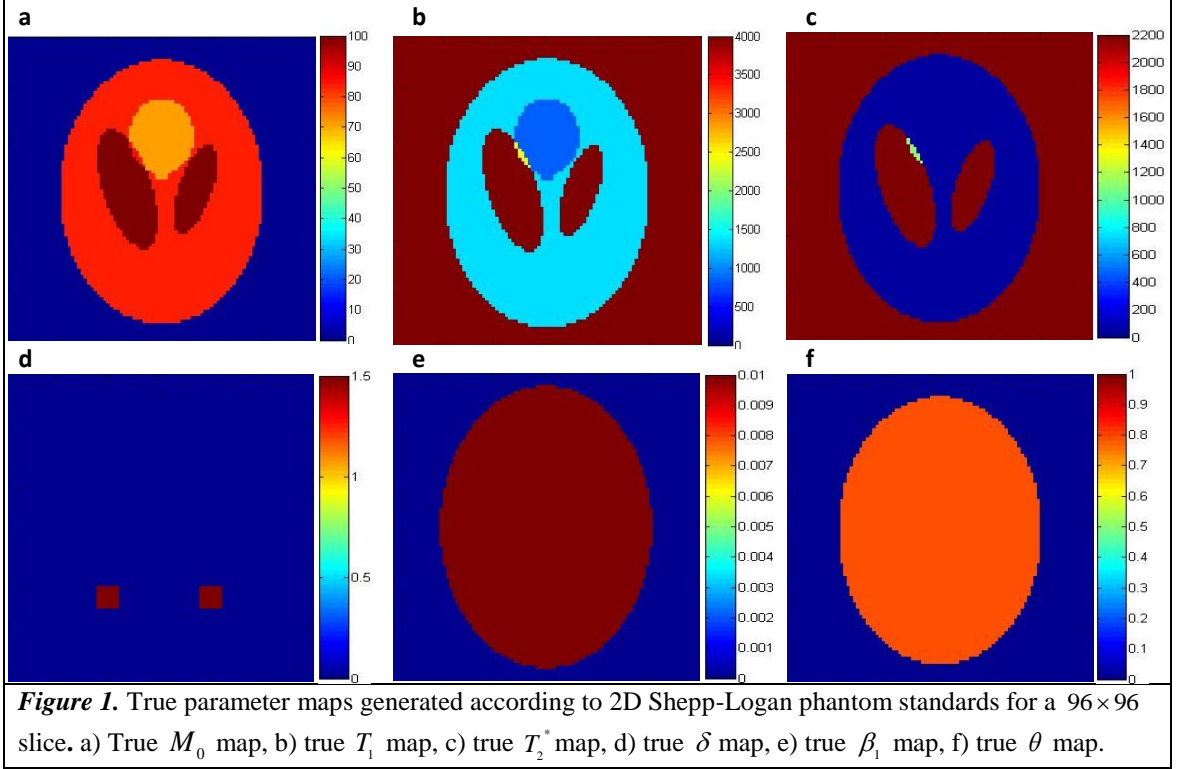
The simulation of the last model consisted of $n = 510$ time points where the true activation structure is known to be within the regions of interest (ROIs) so that the model can be evaluated. A 96×96 slice of the human head with two 7×7 ROIs is realistically simulated according to the Shepp-Logan phantom standards proposed in [2]. The spin density and the relaxation parameter values of the simulated tissues measured at 3.0 Tesla are given in Table 1 [14]. The parameter values of the voxels that consist of different kinds of tissues were obtained by averaging the regarding tissues. For all voxels inside the phantom in this simulation, the phase and the flip angle were generically selected to be $\theta = \pi/4$, $\phi = \pi/4$, while $\beta = .01$ and $\sigma = 1$. The differential T_2^* contrast, δ , was given a constant value of 1.5 for the voxels in ROIs while defined to be zero for the inactive regions.

The presented results in this manuscript are calculated over 50 simulations which are performed using the MATLAB programming language on a dual quad-core PC with 24 gigabytes of RAM running Microsoft Windows 7.

Table 1. Spin Density and the relaxation times in msec for the Shepp-Logan Phantom.

Tissue	M_0	T_1	T_2^*
CSF	100	4000	2200
Gray Matter	83	1331	42
White Matter	71	832	49

The true parameter values are illustrated in Figure 1 for a 96×96 slice of the Shepp-Logan phantom. The maps of the true spin density, M_0 ; longitudinal relaxation, T_1 ; transverse relaxation, T_2^* ; differential T_2^* contrast, δ ; linear trend, β_1 and phase angle, θ are illustrated in Figs. 1a, 1b, 1c, 1d, 1e and 1f, respectively. The voxel relaxivities and proton spin density are different for different tissue types as illustrated in Figs. 1a, 1b and 1c. Two 7×7 ROIs which are lightened in Fig. 1d are designated to have activation. The coefficient for the reference function δ is zero outside the ROIs and has constant value of 1.5 inside each ROI. $\beta_1 = .01$ and $\theta = \pi/4$ are assumed constant across voxels inside the phantom brain whereas they are both zero outside as illustrated in Figs 1e and 1f.



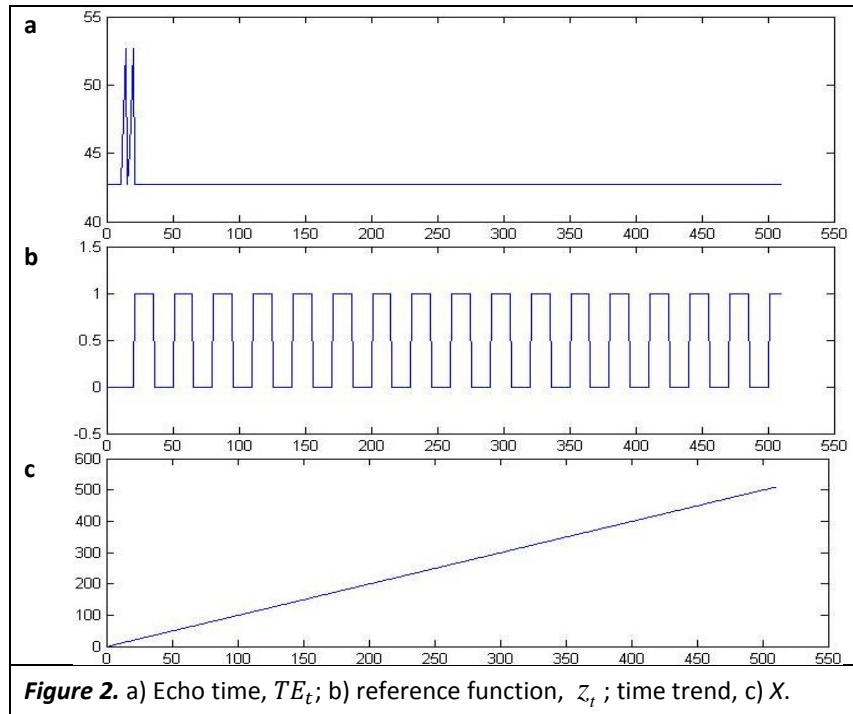
Simulated fMRI data is constructed according to the proposed model given by Eq. (16).

This model dictates that at time t

$$\begin{aligned}
 y_i = & \left\{ \left[\left[M_{t-1} e^{-\frac{TR}{T_1}} \cos(\phi) + M_0 \left(1 - e^{-\frac{TR}{T_1}} \right) \right] \sin(\phi) e^{-\frac{TE_t}{T_2^* + \delta z_t}} + x_t \beta_1 \right] \cos \theta + \eta_{R_t} \right\} \\
 + i & \left\{ \left[\left[M_{t-1} e^{-\frac{TR}{T_1}} \cos(\phi) + M_0 \left(1 - e^{-\frac{TR}{T_1}} \right) \right] \sin(\phi) e^{-\frac{TE_t}{T_2^* + \delta z_t}} + x_t \beta_1 \right] \sin \theta + \eta_{I_t} \right\}, \quad (22)
 \end{aligned}$$

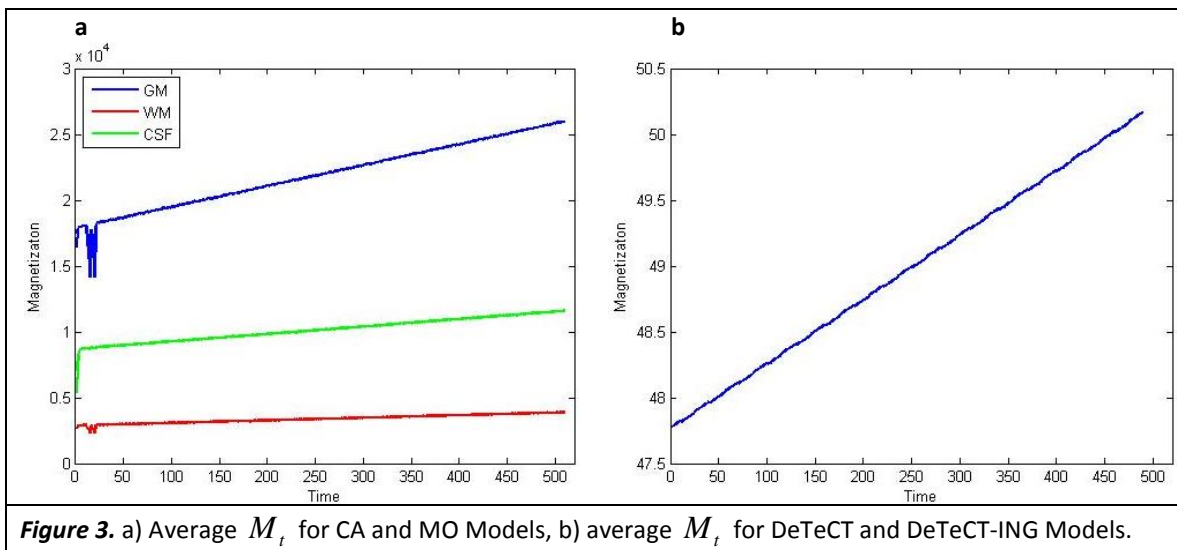
where η_{R_t} and η_{I_t} are independent and identically distributed normal random variables with mean zero and variance σ^2 . For each voxel, time depending echo time, TE_t , is assumed to consist of four parts. It is fixed as having a value of 42.7 at the first 10 time points. Then 5 TE values are equispaced in the interval $[42.7, 52.7]$ and this procedure is repeated again for the next 5 time points. Finally, the last 490 TE values are fixed as 42.7 as illustrated in Fig. 2a. In this simulation,

the time trend X is a column of counting numbers, where the reference function, z_t , consists of blocks of 0's and 1's, as being related to the block experimental design. We illustrate z_t and X in Figs. 2b and 2c, respectively.

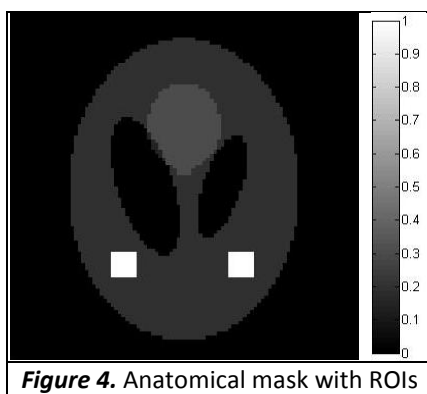


The average effective magnetizations, M_t of each tissue type in the presented models for one simulation are given in Fig. 3. The average M_t for the models CA and MO given in Eq. (3) is illustrated in Fig. 3a, where the average M_t for the models DeTeCT and DeTeCT-ING given in Eq. (16) is illustrated in Fig. 3b. As we noted before, the magnetization follows the linear trend that characterizes the generated fMRI data for both of the model sets. However, the magnetization has different initial values for different tissues in the only DeTeCT and DeTeCT-ING Models, thus the effect of the relaxation parameters on the magnetization can only be seen in Fig. 3b at the first 20 time points. The models CA and MO do not take into the consideration the relaxation parameters and the tissue differences, as we noted before. Furthermore, the first scans which

include the important biological information of the tissues are discarded from the data. Therefore, the magnetization follows the same linear trend regardless of the tissue type for the CA and MO Models as it can be seen in Fig. 3a.



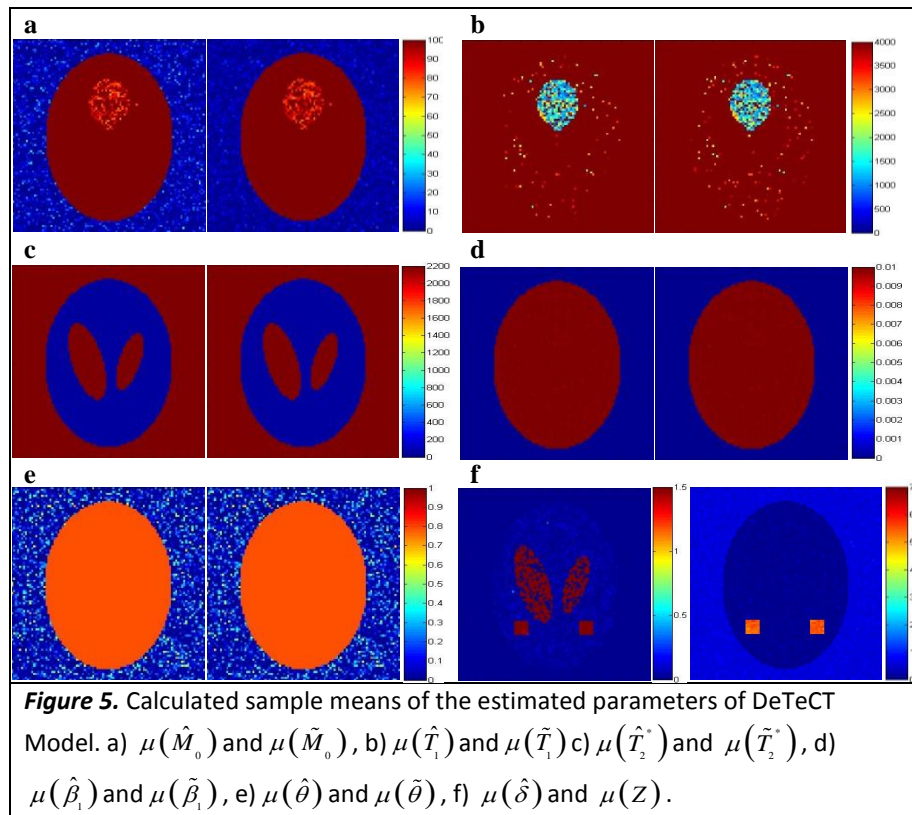
The anatomical mask of the 96×96 2D Shepp-Logan phantom with two ROIs included in gray matter is illustrated in Fig. 4. It can be observed that two ROIs are located symmetrically on both the right and left-hand side of the brain.



The parameter maps of the DeTeCT and DeTeCT-ING Models under the null and the alternative hypothesis given in Eqs. (19) and (21), are estimated by using the nonlinear LS

estimator for each voxel in the considered slice of the phantom. The calculated sample mean and variance of the estimated parameters of the DeTeCT Model under the null and the alternative hypothesis, $H_0 : \delta = 0$ versus $H_1 : \delta \neq 0$, are given in Figs. 5 and 6, respectively. The similarity between the calculated sample means of the parameters, β_1 and θ , given in Figs. 5d and 5e and the true parameter maps given in Figs. 1e and 1f is higher compared to the similarity between the calculated sample means of the parameters, M_0, T_1 and T_2^* , given in Figs. 5a, 5b and 5c and the corresponding true parameter maps given in Figs. 1a, 1b and 1c, respectively. This could possibly be explained as a result of the nonlinear least squares estimation of the parameters M_0, T_1 and T_2^* in Eq. (22) in which the parameter β_1 is linear and θ is a parameter of a trigonometric function. In both the sample mean and sample variance maps of the estimated parameters M_0, T_1, T_2^*, β_1 , and θ , in Figs 5a-5d, 5f there appears to be a poor estimation of those parameters in some tissues such as CSF. This is the result of having a nonlinear objective function given in Eq. (18) and six different parameters to be optimized in this system. The differences in the parameters in different tissues which are not taken into the consideration in CA and MO Models can be considered as another reason of that result. As previously noted, statistically significant task-related activation was detected using a 5% Bonferroni family-wise-error rate (FEW). The mean of the differential coefficient for the reference function δ and the Z statistics map calculated by using a 5% FWE given in Eq. (8) are illustrated in Fig. 5f. (A map of estimated values for δ under the null hypothesis is not shown as it is all zeros.) One can observe that the DeTeCT Model which uses the complex-valued measurements can detect task-related changes as can be seen by the highly active square ROIs in the Z map of Fig 5f. (right). The high δ values in CSF in Fig. 5f (left) could possibly be explained by the nonlinear least squares estimation of that parameter, similarly with the parameters M_0, T_1 and T_2^* in Eq. (22).

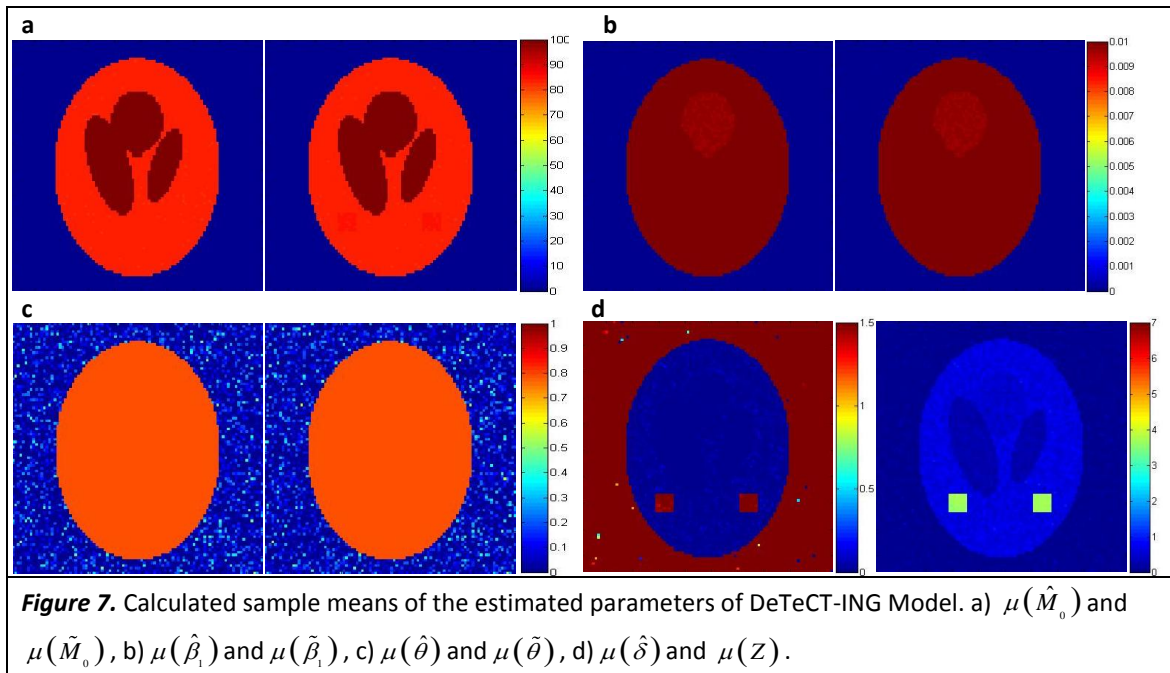
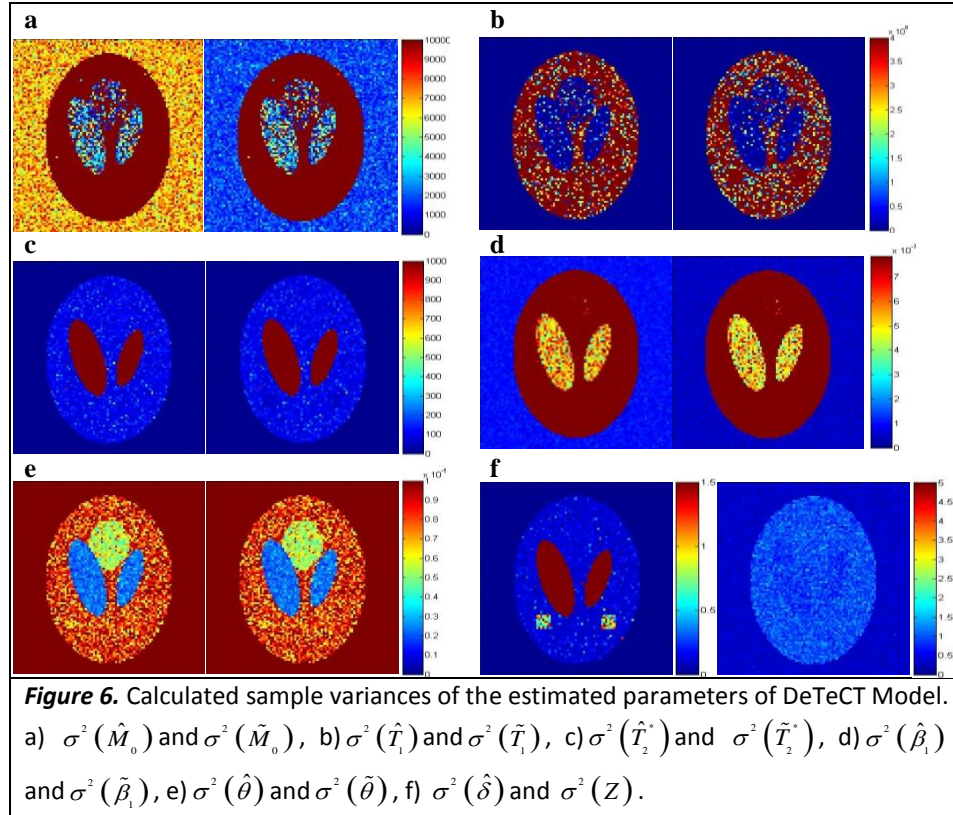
The sample variances of the estimated parameters M_0, T_1, T_2^*, β_1 and θ , under the null and the alternative hypothesis appear to be similar to each other as illustrated in Figs 6a-6e. However, one can see that the sample variance of the estimated M_0 under the alternative hypothesis given in Fig. 6a (left) is higher outside the phantom brain compared to the sample variance of the estimated M_0 under the null hypothesis given in Fig. 6b (right). A similar result can also be observed in the sample variance of the parameter β_1 outside the phantom brain as illustrated in Fig. 6d. There is a slight difference in the sample variances outside the phantom brain as it can be seen in Fig. 6d (left) and Fig. 6d (right). (A map of estimated variances for δ under the null hypothesis is not shown as it is all zeros.)



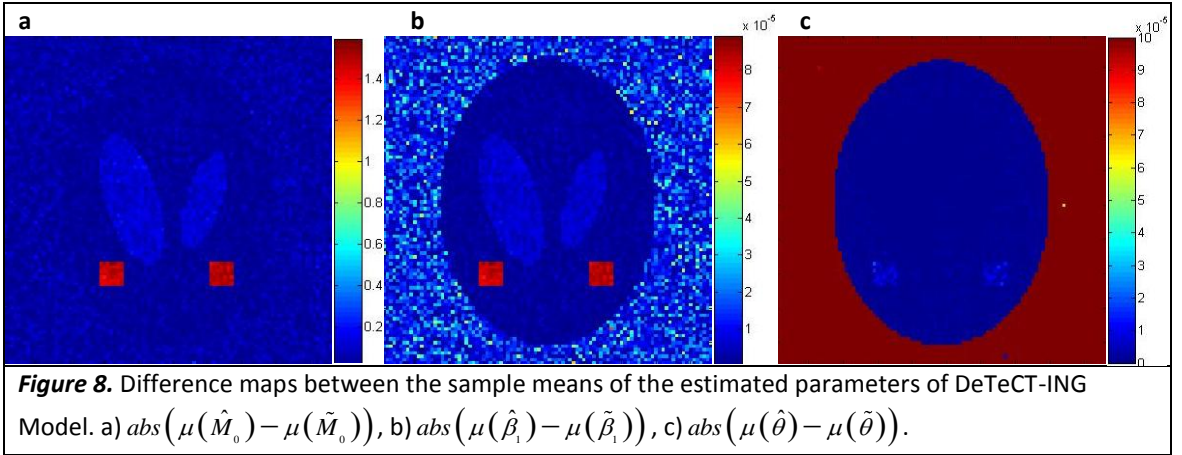
Similarly with the DeTeCT Model, the parameters of the DeTeCT-ING Model, estimated under the null and the alternative hypothesis, $H_0 : T_1 = T_{1_{GM}}, T_2^* = T_{2_{GM}}^*, \delta = 0$ versus

$H_1 : T_1 = T_{1_{GM}}, T_2^* = T_{2_{GM}}^*, \delta \neq 0$, are illustrated in Figs. 7 and 9, respectively.

Figs. 7a-7d (left) show that the calculated sample means of the parameters M_0, β_1, θ and δ , under both the alternative and the null hypotheses appear to be similar to the corresponding true parameter maps given in Figs 1a, 1d-f. (A map of estimated values for δ under the null hypothesis is not shown as it is all zeros.) However, in white matter tissue, the value of the parameters, M_0 and β_1 which are given in Figs. 7a and 7b appear to be different than the corresponding true values of those parameters given in Figs. 1a and 1b, respectively. Also, the value of the parameter δ given in Fig. 7d is higher outside the phantom brain compared to its true value given in Fig. 1d (left). Similarly with the DeTeCT Model, the DeTeCT-ING Model can detect task-related changes in ROIs as illustrated in Fig. 7d (left) which shows the statistically significant difference in the δ values within the ROIs and in Fig 7d (left) which gives higher activation statistics in those regions compared to the other areas in the phantom brain.



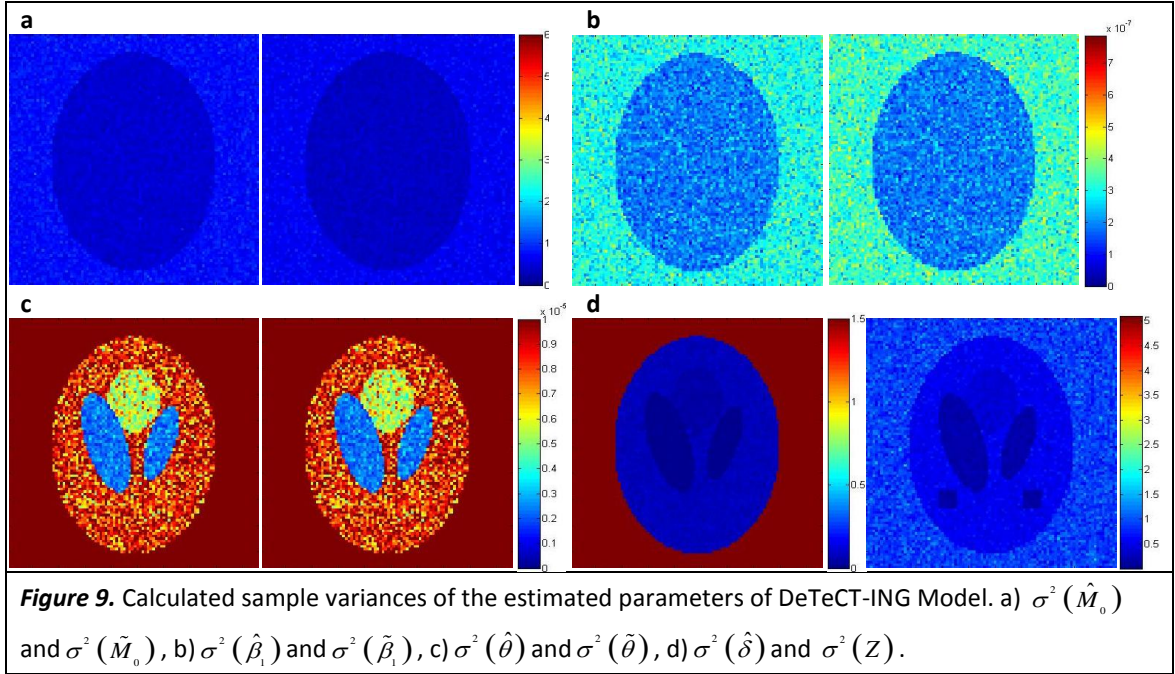
To better illustrate the differences between the null and the alternative hypothesis estimation, we present the corresponding difference maps for M_0 , β_1 , and θ in Figs. 8a-8c. Difference maps in Fig. 8a and Fig. 8b indicate that the most apparent difference in all parameters inside the phantom brain occurs in the ROIs since the only difference in the hypothesis setting given in Eq. (21) is in those regions. In Fig. 8b, the difference map indicates that the difference in the estimation of the parameter, β_1 under the null and the alternative hypothesis increases outside the phantom brain. The difference maps also show a large difference in the estimated phase θ outside the phantom in Fig. 8c.



The parameters M_0 , β_1 , θ , and δ , estimated in DeTeCT-ING Model shown in Figs. 9a-9d appear to have lower sample variances compared to those estimated in Figs. 6a and 6d-f for the DeTeCT Model. This decreased variance is a result of having fewer parameters to be estimated according to the hypothesis pair given in Eq. (21) in which at least two parameters are set to constant values.

The variability in the estimated parameter map images is the result of the noise in the signal as well as the systematic error of the numerical optimization procedure. In areas without signal, such as outside of the phantom brain, have not been masked after estimation. Thus, the

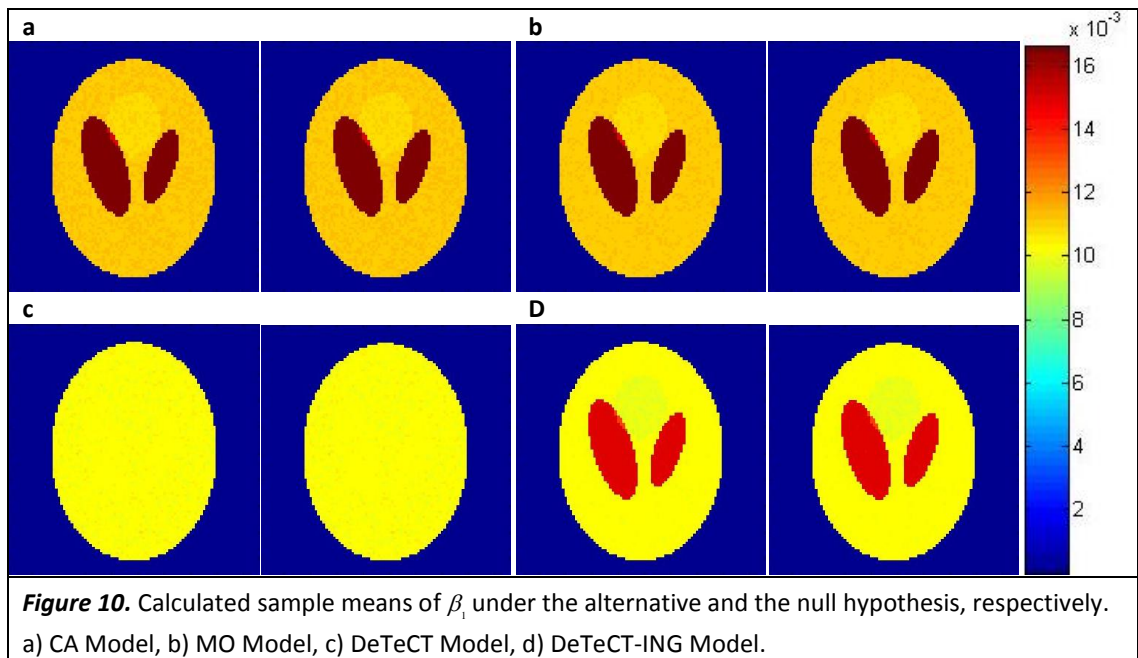
parameters for the voxels which are outside of the phantom brain may not have been estimated precisely as we would expect. It should also be noted here that the results of the numerical optimization process would yield more accurate results as we increase the number of the simulated experiments that have been done. The similar result is to be expected if the standard deviation of the noise is decreased.



To better illustrate the observed results for our new models, we compare the sample mean and variances of the parameters which are estimated by using the CA, MO, DeTeCT and DeTeCT-ING Models. For all of the models, we used the same data which have been generated by Eq. (16) that takes into account the physical magnetization as in real case. We present the descriptive statistics of the parameters, β_1 , which is one of the two parameters that are estimated in all of the models under the null and the alternative hypothesis.

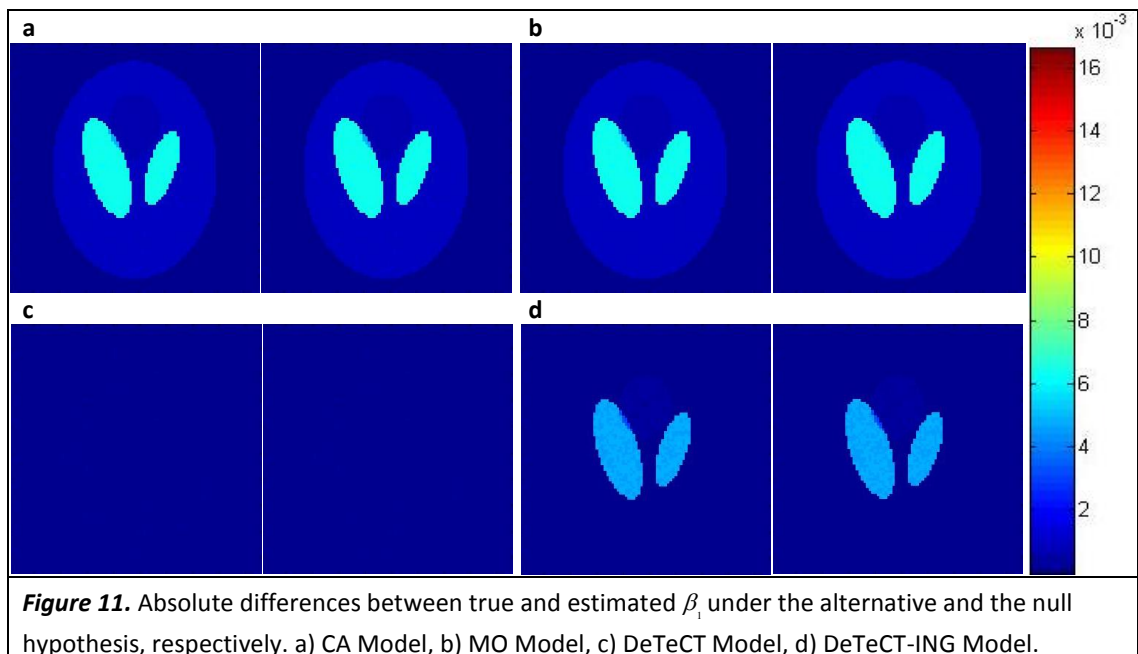
Calculated sample means of β_1 under the alternative and null hypothesis according to CA and MO Models appear to be similar and have higher values in CSF areas as illustrated in

Figs. 10a and 10b. Note that, the CA and MO models assume a linear model to represent the magnetization over time and do not consider that the true form of the magnetization, and thus the signal is different in different tissues. The generated data using the true physical magnetization in Eq. 16, introduced in models DeTeCT and DeTeCT-ING, mimics the known truth for fMRI data better than the linear magnetization representation in the CA and MO models. As a result of this, the sample mean of the parameter β_1 estimated according to DeTeCT and DeTeCT-ING Models shown in Figs. 10c and 10d produce better results than for the CA and MO models as can be observed in Figs. 10a and 10b.

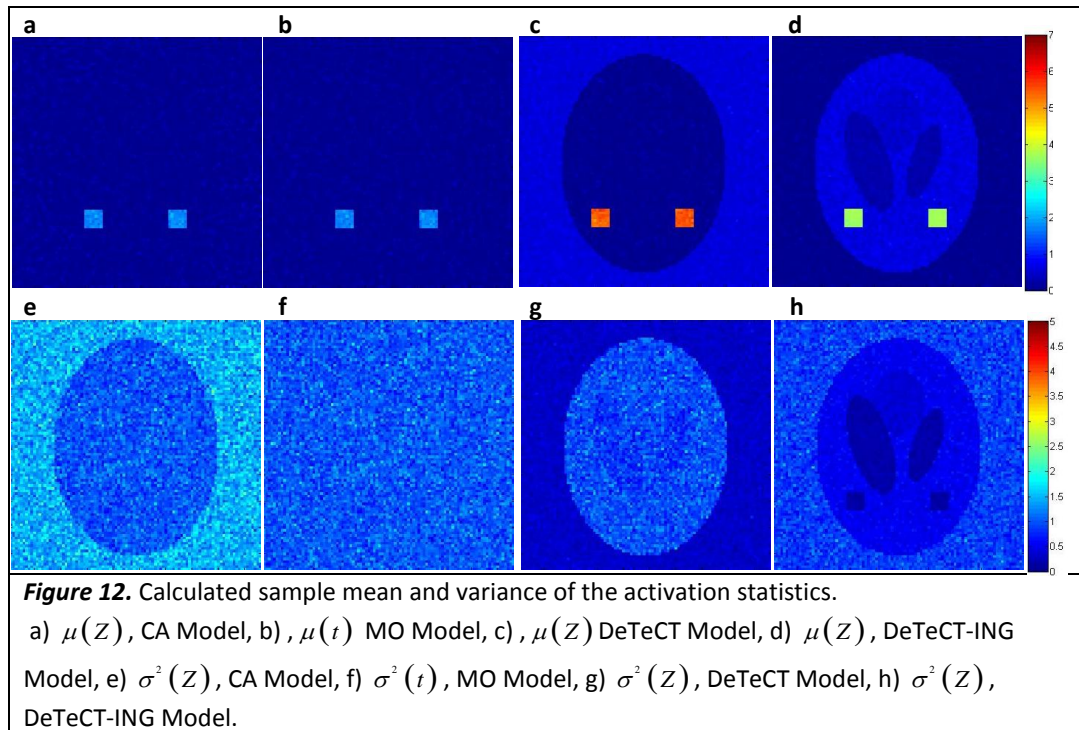


The absolute differences between true β_1 map given in Fig. 1e and the sample mean of the estimated β_1 according to the models given in Figs. 10a-d are illustrated in Fig. 11. It is obvious that estimation of β_1 is better when it is done by using DeTeCT and DeTeCT-ING Models as can be seen in Figs. 11c and 11d as compared to Figs. 11a and 11b.

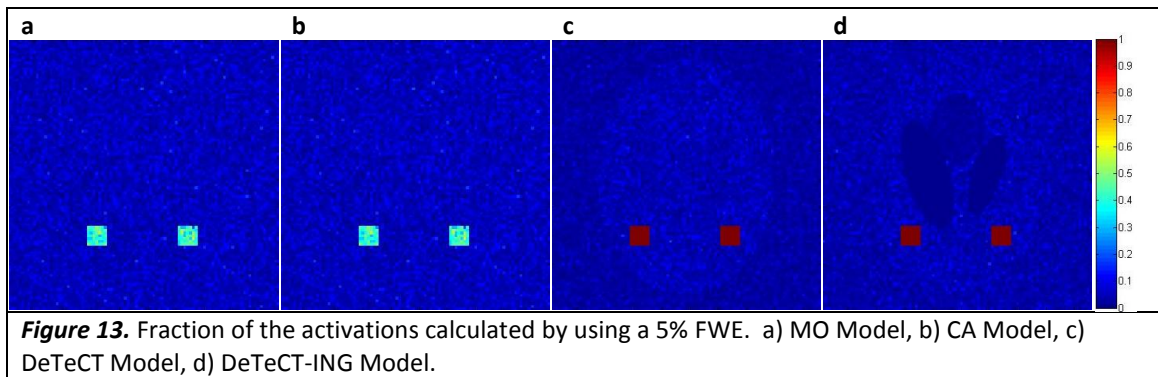
The activation statistics are computed from a generalized likelihood ratio test for the models which use the complex-valued voxel observations (CA, DeTeCT and DeTeCT-ING Models) and the one which uses the magnitude of the complex-valued observations (MO Model), by using the Eqs. (8) and (15), respectively. In Figs. 12a-h, we present the calculated sample mean and sample variances of the activation statistics maps of the models CA, MO, DeTeCT and DeTeCT-ING. One can observe that the sample mean of the activation statistics of the CA and MO Models given in Figs. 12a and 12b is higher than those of the DeTeCT and DeTeCT-ING Models given in Figs. 12c and 12d. It is evident that inside the phantom brain, the lowest sample variance in activation statistics appears to be in DeTeCT-ING Model illustrated in Fig. 12h compared to the sample variance of the models CA, MO and DeTeCT, given in Figs. 12e, 12f and 12g, respectively. This result shows that the proposed activation setting in DeTeCT-ING Model is better in detecting the fMRI activation comparing to the other models. It can also be seen that the sample variance of the CA Model given in Fig. 12e is lower outside the phantom brain compared to the sample variance of the MO Model illustrated in Fig. 12f.



Moreover, the sample variance of the DeTeCT Model given Fig. 12g is lower outside the phantom compared to both models CA and MO whose activation statistics' sample variances are given in Figs 12e and 12f, respectively.



As previously noted, statistically significant task-related activation for each of the models was detected using a 5% Bonferroni FWE rate. The voxels above the threshold for the models are detected as “active” voxels, whereas the voxels below the threshold are detected as “inactive”. The fraction of the activations of the models, CA, MO, DeTeCT and DeTeCT-ING calculated over 50 simulations are illustrated in Figs. 13a, 13b, 13c, and 13d, respectively. By comparing the fraction of the activations calculated by using MO and CA Models in Figs. 13a and 13b, to those calculated by DeTeCT and DeTeCT-ING Models in Figs. 13c and 13d; it is evident that 100% of the time, DeTeCT and DeTeCT-ING Models are able to detect the activation which was assumed to be in ROIs. The fraction of the activation calculated by the models CA and MO is around 0.5; whereas it is exactly 1 when the DeTeCT and DeTeCT-ING Models are used.



5. DISCUSSION

A statistical fMRI model for differential T_2^* contrast, so called the DeTeCT-ING Model, was developed by incorporating T_1 and T_2^* of gray matter tissue, considering the fact that the active voxels are located in gray matter, the part of the brain that contains neural cell bodies, due to the relatively greater blood flow and volume in there. Furthermore, the physical magnetization equation was included into the model rather than using a linear model to describe the magnetization which is a common practice in previous studies.

Activation statistics were numerically evaluated from the maximum likelihood estimates of the model parameters including differential T_2^* contrast for a simulated data set. Unlike the previously presented fMRI activation models, we did not exclude the first few images from the data since the first scans of the stationary tissue still have the biological information of the brain, including the tissue parameters such as relaxation parameter and spin density of the tissues.

There are two main contributions of the developed model to the current studies in the field by utilizing the neglected information as we noted above: Simultaneous estimation of the model parameters would be a practical method for the well-known process of detecting activation in fMRI; and constructing hypothesis tests by incorporating T_1 and T_2^* of gray matter would

provide more significant activation statistics. The model would also allow one to estimate the tissue and the imaging parameters which could be used for tissue characterization, by utilizing the information in the first few images.

The next direction of this work would be applying the proposed model to the real fMRI data which is gathered by using the same system parameter values such as repetition time, echo time and the flip angle as we have used in our simulations.

BIBLIOGRAPHY

- [1] Baselice, F., Ferraioli G. & Pascazio, V. Relaxation time estimation from complex magnetic resonance imaging. *Sensors*. 2010;10, 3611-3625.
- [2] Gach, H. M., Tanase, C., Boada, F. 2D & 3D Shepp-Logan phantom standards for MRI. *ICSENG '08. 19th International Conference on Systems Engineering*. 2008; 521-526.
- [3] Haacke, E.M., Brown, R., Thompson, M., Venkatesan, R. *Magnetic resonance imaging: physical principles and sequence design*. New York, NY, USA: John Wiley and Sons 1999.
- [4] Mazaheri, Y., Biswal, B. B., Ward, B. D. & Hyde, J. Measurements of tissue T1 spin-lattice relaxation time and discrimination of large draining veins using transient EPI data sets in BOLD-weighted fMRI acquisitions. *NeuroImage*. 2006;32,603-615.
- [5] Ogawa S., Lee T. M., Kay, A. R., Ellermann, J. M., Kim, S. G., Merkle, H & Ugurbil, K. Intrinsic signal changes accompanying sensory stimulation: Functional brain mapping with magnetic resonance imaging. *Proceedings of the National Academy of Sciences of the United States of America*. 1992;89,5951-5955.
- [6] Ogawa, S., Lee, T. M., Kay A. R., Tank, D. W. Brain magnetic resonance imaging with contrast dependent on blood oxygenation. *Proc. Natl. Acad. Sci*. 1990;87, 9868-9872.
- [7] Rowe, D. B. Parameter estimation in the magnitude-only and complex-valued fMRI data models. *NeuroImage*. 2005;25,1124-1132.
- [8] Rowe, D.B., Logan, B.R. A complex way to compute fMRI. *NeuroImage*. 2004;23(3), 1078-1092.
- [9] Gudbjartsson, H., Patz, S. The Rician distribution of noisy data. *Magn. Reson. Med*. 1995;34(6), 910-914.
- [10] Larkman, D.J., Nunes, R.G. Parallel magnetic resonance imaging. *Phys Med. Biol*. 2007;52,15-55.
- [11] Bandettini, P., Jesmanowicz, A., Wong, E., Hyde, J.S. Processing strategies for time-course data sets in functional MRI of the human brain. *Magn. Reson. Med*. 1993;30(2),161-173.
- [12] Cox, R.W., Jesmanowicz, A., Hyde, J.S. Real-time functional magnetic resonance imaging. *Magn. Reson. Med*. 1995;33(2),230-236.
- [13] Severini, T.A. *Likelihood Methods in Statistics*. Oxford, UK: Oxford University Press 2001.
- [14] Atlas, S. W. *Magnetic Resonance Imaging of the Brain and Spine, Fourth Edition, Volume 1*. Philadelphia, USA: Lippincott Williams & Wilkins 2008.

- [15] Bandettini, P., Jesmanowicz, A., Wong, E., Hyde, J.S. Processing strategies for time-course data sets in functional MRI of the human brain. *Magn. Reson. Med.* 1993;30(2),161-173.
- [16] Rowe DB, Logan BR. Complex fMRI analysis with unrestricted phase is equivalent to a magnitude-only model. *Neuroimage.* 2005;24:603-606.
- [17] Logan BR., Rowe DB. An evaluation of thresholding techniques in fMRI analysis. *Neuroimage.* 2004;22(1):95-108.

Marquette University

This is to certify that we have examined this copy of the thesis by

M. Muge. Karaman

and have found that it is complete and satisfactory in all respects.

This thesis has been approved by:

Dr. Daniel B. Rowe, Department of Mathematics, Statistics, and Computer Science

Approved on
